General Model for Dissolution Rates of n-Component, Nondisintegrating Spheres

G. R. CARMICHAEL *, S. A. SHAH ‡§, and E. L. PARROTT ‡x

Received January 9, 1981, from the *Chemical and Materials Engineering Program and the ‡Division of Pharmaceutics, College of Pharmacy, University of Iowa, Iowa City, IA 52242. Accepted for publication April 7, 1981. §Present address: Zenith Laboratories, Northvale, NJ 07646.

Abstract □ The dissolution rates of compressed spheres consisting of two and three components were measured. A general model for dissolution rates of n-component, nondisintegrating spheres is discussed. Experimental cases are presented to support the model for two- and three-component spheres, two-component interacting spheres, and three-component spheres containing two components that complex.

Keyphrases □ Dissolution—general model for n-component, nondisintegrating spheres □ Spheres—n-component, nondisintegrating, general model for dissolution rates □ Models, dissolution—for n-component, nondisintegrating spheres

Few studies on dissolution rates have involved multicomponent solids. One early study (1) involving the dissolution of a two-component system examined the dissolution rates of several poorly soluble weak acids and tribasic sodium phosphate in various mole fractions. The dissolution rates of salicylic acid and povidone from compressed disks also were reported (2). Diffusion models also were suggested (3) for the dissolution of nondisintegrating multicomponent mixtures containing noninteracting components and complexing components. Shah and Parrott (4) applied the model to the dissolution of four two-component solids.

This study presents a general model for the dissolution rates of a nondisintegrating sphere containing any number of components. The model was developed from the viewpoint of mass transfer, and experimental cases are presented demonstrating its application to two- and three-component solids, two-component interacting solids, and three-component solids with two components interacting.

THEORY

A model for the dissolution rate of a spherical solid particle may be described assuming that (*a*) the dissolution rate is diffusion controlled, (*b*) the diffusion layer thickness is always the same for all particles of the same size, (*c*) the concentration change of the dissolved solid in the dissolution medium is negligible, (*d*) the effective particle shape approximates a sphere, and (*e*) the initial solid composed of n components is homogeneous.

From the viewpoint of mass transfer, if multicomponent diffusion effects are ignored, the change in mass with time, dW_i/dt, of a noninteracting component in the solid can be expressed as:

$$\frac{dW_i}{dt} = -k_i S_i (C_i^* - C_i) \qquad \text{(Eq. 1)}$$

where k_i is the liquid phase mass transfer coefficient, S_i is the surface area available for mass transfer, and C_i^* and C_i are the interfacial and bulk mass concentrations of species in the liquid phase, respectively, for components $i = 1$ to n. Since the surface area of a sphere is $4\pi r^2$, Eq. 1 may be written as:

$$\frac{dW_i}{dt} = -k_i 4\pi r_i^2 (C_i^* - C_i) \qquad \text{(Eq. 2)}$$

The mass of a given component in the solid is related to the volume of the particle, the mass fraction, X_i, and the bulk density, ρ. Since:

$$W_i = \frac{4}{3}\pi r_i^3 X_i \rho \qquad \text{(Eq. 3)}$$

and if X_i is not a function of time, Eq. 2 may be written as:

$$-\frac{dr_i}{dt} = \frac{D_i (C_i^* - C_i)}{h X_i \rho} \qquad \text{(Eq. 4)}$$

where, for diffusion-controlled dissolution in which there is no chemical reaction, the liquid phase mass transfer coefficients are expressed in terms of diffusion coefficients, D_i, and the film thickness, h.

As dissolution proceeds, the more soluble components dissolve faster and are depleted near the solid–liquid interface, resulting in a surface layer composed of the least soluble component. At any time, the solid is conceptualized as consisting of a homogeneous core with the initial composition, an outer shell of the least soluble component, and, between them, $n - 2$ concentric layers comprised of components of intermediate solubilities. If the nth component is the least soluble component, Eq. 4 may be written as:

$$-\frac{dr_n}{dt} = \frac{D_n}{X_n h \rho}(C_n^* - C_n) \qquad \text{(Eq. 5)}$$

and:

$$-\frac{dr_i}{dt} = \frac{D_i (C_i^* - C_i)}{(h + r_n - r_i) X_i \rho} \qquad \text{(Eq. 6)}$$

where h is the film thickness and $(h + r_n - r_i)$ includes an internal diffusion thickness (or resistance) of $r_n - r_i$.

Equations 2, 5, and 6 may be used to calculate the dissolution rates of n-component solids. The fluxes, J_i, may be found from the equations:

$$J_i = \frac{1}{S_n}\frac{dW_i}{dt} = -k_i \frac{S_i}{S_n}(C_i^* - C) \qquad \text{(Eq. 7)}$$

and:

$$J_n = \frac{1}{S_n}\frac{dW_n}{dt} = -k_n (C_n^* - C_n) \qquad \text{(Eq. 8)}$$

where the fluxes are normalized in terms of the external surface area, S_n, of the solid.

The weight of the solid at any time can be calculated from:

$$W = \sum_{i=1}^{n} W_i \qquad \text{(Eq. 9)}$$

These equations will be used to model the dissolution of two- and three-component solids. In addition, these equations can be modified to include cases with interaction between the components.

EXPERIMENTAL

Preparation of Compressed Spheres and Measurement of Densities—Material that passed through an 80-mesh sieve but was retained on a 100-mesh sieve was compacted at 4540 kg of force, by means of a hydraulic press[1], into compressed spheres having a diameter of 1.270 ± 0.005 cm. The bulk density of the compressed spheres was determined by displacement (4). The true density of the material was determined by means of a pycnometer using n-heptane.

Dissolution Rate—The dissolution rate was determined in distilled water at 25 ± 0.1°, as described previously (5, 6), under conditions where the concentration of the solutes did not exceed 5% of solubility. The dissolution apparatus and procedure were described previously (4, 6), and the dissolution rates are given in Tables I and II.

Analytical Procedures—The simultaneous analysis of two-compo-

[1] Carver press, model C.

Table I—Composition and Experimental Dissolution Rates of Two-Component Solids Compressed at 4540 kg

Mole Fraction		Dissolution Rate, g/hr/cm²		
		Aspirin–Salicylic Acid		
X_{ASA}	X_{SAL}	ASA	SAL	Sphere
1.0	0	0.0430	—	0.0430
0.9	0.1	0.0423	0.0036	0.0459
0.8	0.2	0.0415	0.0080	0.0495
0.7	0.3	0.0382	0.0125	0.0507
0.6	0.4	0.0336	0.0171	0.0507
0.5	0.5	0.0282	0.0216	0.0498
0.4	0.6	0.0215	0.0248	0.0463
0.3	0.7	0.0148	0.0264	0.0412
0.2	0.8	0.0088	0.0271	0.0359
0.1	0.9	0.0039	0.0272	0.0311
0	1.0	—	0.0272	0.0272
		Aspirin–Phenacetin		
X_{ASA}	X_{PH}	ASA	PH	Sphere
1.0	0	0.0430	—	0.0430
0.9	0.1	0.0370	0.0041	0.0411
0.8	0.2	0.0320	0.0079	0.0399
0.7	0.3	0.0269	0.0115	0.0384
0.6	0.4	0.0195	0.0129	0.0324
0.5	0.5	0.0130	0.0125	0.0255
0.4	0.6	0.0081	0.0120	0.0201
0.3	0.7	0.0051	0.0120	0.0171
0.2[a]	0.8	0.0025	0.0098	0.0123
0.1[b]	0.9	0.0010	0.0086	0.0096
0	1.0[b]	—	0.0080	0.0080

[a] Compressed at 680 kg. [b] Melt method.

nent spheres of aspirin (ASA) and salicylic acid (SAL), and of aspirin and phenacetin (PH), and of three-component spheres of aspirin, caffeine (CAF), and phenacetin using simultaneous equations was discussed previously (4, 7).

RESULTS AND DISCUSSIONS

Two-Component, Noninteracting Solids—Two systems (aspirin–salicylic acid and aspirin–phenacetin) were studied. The experimental dissolution rates for various compositions of both systems are given in Table I. The solubilities and diffusion coefficients used in the calculations are compiled in Table III. The weight of the spheres and the fluxes (dissolution rates) were calculated from Eqs. 1 and 5–9. These equations were solved simultaneously using a fourth-order Runge–Kutta procedure (8).

For example, at 2 hr, the theoretical predicted weights are compared to the experimentally determined weights for aspirin–salicylic acid spheres in Fig. 1 and for aspirin–phenacetin spheres in Fig. 2. The predicted weights are within 6% of the determined weights, and the calculated values indicate that the maximum loss of weight occurs at an intermediate value of X_{ASA}.

Table III—Physical Parameters of Species in Water at 25°

Material	D_i, cm²/sec	C_i^* g/ml
Aspirin	8.01×10^{-6} [a]	4.44×10^{-3} [a]
Salicylic acid	10.12×10^{-6} [b]	2.24×10^{-3} [c]
Caffeine	6.79×10^{-6} [d]	23.2×10^{-3} [e]
Phenacetin	9.0×10^{-6} [f]	1.1×10^{-3} [g]
Aspirin–caffeine complex	6.79×10^{-6} [h]	—

[a] L. J. Edwards, *Trans. Faraday Soc.*, **47**, 1191 (1951). [b] J. W. Mullin and T. P. Cook, *J. Appl. Chem.*, **15**, 145 (1965). [c] N. A. Halla, *Am. J. Pharm.*, **132**, 406 (1960). [d] M. McCabe, *Biochem. J.*, **127**, 249 (1972). [e] A. N. Paruta, B. J. Sciarrone, and N. G. Lordi, *J. Pharm. Sci.*, **54**, 838 (1965). [f] C. D. Shively and D. O. Kildsig, *ibid.*, **61**, 1589 (1972). [g] A. Seidell, *J. Am. Chem. Soc.*, **92**, 1088 (1970). [h] Assumed to be the same as caffeine.

The general model predicts that maximum dissolution rates occur for composite solids in which there is no internal diffusion resistance (all the r_i values are equal). This critical composition can be found by equating the right-hand sides of Eq. 6 with $r_n = r_i$ and $C_i = 0$; thus:

$$\frac{D_1 C_1^*}{hX_1\rho} = \frac{D_2 C_2^*}{hX_2\rho} \qquad \text{(Eq. 10)}$$

which can be rearranged to:

$$\frac{X_2}{X_1} = \frac{D_2 C_2^*}{D_1 C_1^*} \qquad \text{(Eq. 11)}$$

where $X_1 + X_2 = 1$.

In general, the r_i values of the dissolving components are not equal and may vary with time. For example, in Fig. 3 the radius is plotted *versus* time for different initial compositions of aspirin and phenacetin. Where $X_{ASA} = 0.1$ and phenacetin comprises the outer shell, the external radius of the solid varies linearly with time while the radius of the homogeneous core varies nonlinearly. In Fig. 3, the internal diffusion thickness for aspirin is dependent on time. For the critical composition of the solid, the internal resistance is zero and $r_{ASA} = r_{PH}$.

Since the internal diffusion thickness is dependent on time, the fluxes are also time variant (Eqs. 7 and 8). Examples of this situation are shown in Fig. 4 for an aspirin–salicylic acid sphere with $X_{ASA} = 0.2$ and for aspirin–phenacetin spheres with $X_{ASA} = 0.2$ and 0.7. Since there is no internal resistance at $t = 0$, the fluxes have their maximum value; subsequently, the flux of the more soluble component decreases as the internal resistance is increased. The average flux, $\bar{J}$, may be calculated by:

$$\bar{J} = \frac{\int_0^t J(t)\,dt}{\int_0^t dt} \qquad \text{(Eq. 12)}$$

At 2 hr, the theoretical average fluxes of aspirin and salicylic acid were calculated and plotted in Fig. 5 for the aspirin–salicylic acid spheres of various composition. The symbols represent the experimental values. Similarly, the average fluxes of aspirin and of phenacetin are plotted *versus* composition in Fig. 6 for comparison to theoretical values.

Table II—Composition and Experimental Dissolution Rates of Three-Component, Interacting System

Mole Fraction			Density,	Dissolution Rate[a], g/hr/cm²			
X_{ASA}	X_{PH}	X_{CAF}	g/cm³	ASA	PH	CAF	Sphere
0.4	0.2	0.4	1.46	0.0650	0.0323	0.0701	0.1674
				0.0679	0.0338	0.0733	0.1750
0.25	0.5	0.25	1.39	0.0077	0.0154	0.0083	0.0314
				0.0079	0.0158	0.0085	0.0322
0.167	0.667	0.167	1.35	0.0026	0.0106	0.0029	0.0161
				0.0026	0.0105	0.0028	0.0159
0.4	0.4	0.2	1.41	0.0167	0.0166	0.0090	0.0423
				0.0165	0.0164	0.0089	0.0418
0.25	0.25	0.5	1.42	0.0452	0.0451	0.0975	0.1878
				0.0446	0.0444	0.0961	0.1851
0.167	0.167	0.667	1.43	0.0495	0.0492	0.2127	0.3114
				0.0454	0.0452	0.1952	0.2853
0.2	0.4	0.2	1.37	0.0160	0.0319	0.0345	0.0824
				0.0169	0.0338	0.0365	0.0872
0.5	0.25	0.25	1.45	0.0368	0.0183	0.0198	0.0749
				0.0362	0.0180	0.0196	0.0738
0.667	0.167	0.167	1.47	0.0417	0.0104	0.0113	0.0634
				0.0409	0.0102	0.0111	0.0622
0.333	0.333	0.333	1.43	0.0290	0.0289	0.0313	0.0892

[a] Two determination for each composition.

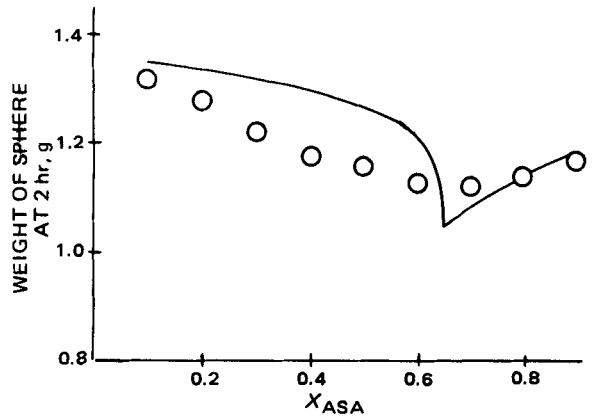

Figure 1—*Relation of composition to weight of a dissolving aspirin–salicylic acid sphere having a bulk density of 1.52 g/cm³. Smooth curve is theoretical, and points are experimental values.*

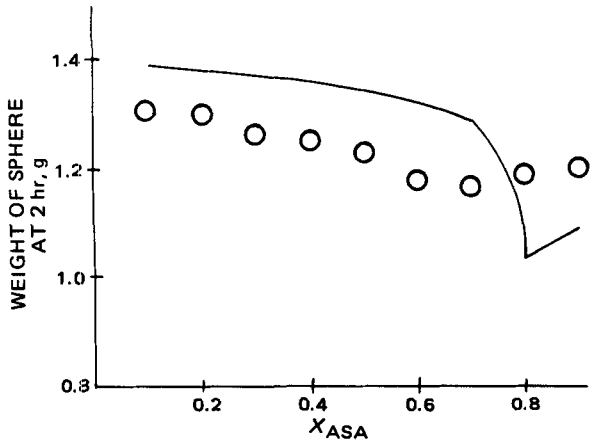

Figure 2—*Relation of composition to weight of a dissolving aspirin–phenacetin sphere having a bulk density of 1.42 g/cm³. Smooth curve is theoretical, and points are experimental values.*

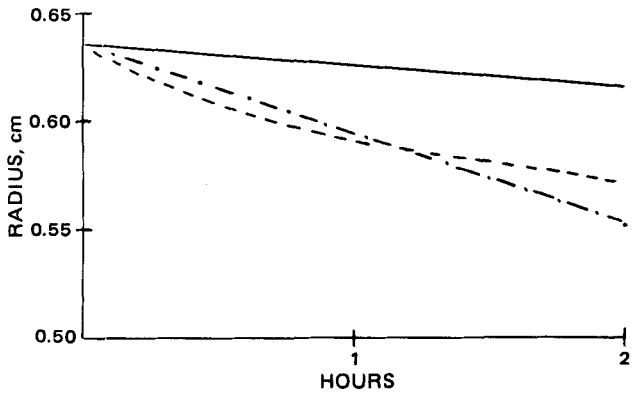

Figure 3—*Radius of layers of the components of a dissolving aspirin–phenacetin sphere with a bulk density of 1.42 g/cm³ as a function of time at the critical composition and at X_{ASA} = 0.1. Key: —, r_{PH} at X_{ASA} = 0.1; ---, r_{ASA} at X_{ASA} = 0.1; and —·—, r_{PH} = r_{ASA} at X_{ASA} = 0.8.*

Three-Component, Noninteracting Solids—For three-component, noninteracting solids, the critical composition is found from:

$$\frac{D_1C_1^*}{hX_1\rho} = \frac{D_2C_2^*}{hX_2\rho} = \frac{D_3C_3^*}{hX_3\rho} \qquad \text{(Eq. 13)}$$

or:

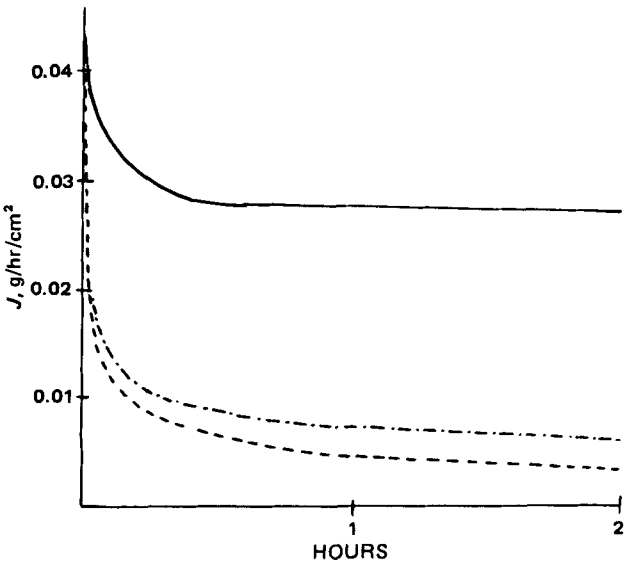

Figure 4—*Instantaneous flux from two-component spheres as a function of time. Key: —, J_{PH} at X_{ASA} = 0.7 and X_{PH} = 0.3 with a bulk density of 1.42 g/cm³; ---, J_{ASA} at X_{ASA} = 0.2 and X_{PH} = 0.8 with a bulk density of 1.42 g/cm³; and —·—, J_{ASA} at X_{ASA} = 0.2 and X_{SAL} = 0.8 with a bulk density of 1.46 g/cm³.*

$$\frac{X_2}{X_1} = \frac{D_2C_2^*}{D_1C_1^*} \qquad \text{(Eq. 14)}$$

$$\frac{X_2}{X_3} = \frac{D_2C_2^*}{D_3C_3^*} \qquad \text{(Eq. 15)}$$

where $X_1 + X_2 + X_3 = 1$.

For the argument of model comparison, no interaction is assumed to occur in the dissolution of an aspirin–caffeine–phenacetin solid. With this assumption, the average fluxes for the components were calculated and plotted in Fig. 7 at X_{PH} = 0.5. For X_{PH} values greater than ~0.1, the phenacetin is the outer shell, and the flux of phenacetin is constant for all X_{ASA} values. For X_{PH} of < 0.1, either the caffeine or the aspirin can be the outer shell, depending on the composition. As shown in Fig. 8 at X_{PH} = 0.05, if $X_{ASA} \geq 0.2$, aspirin is the outer shell, and if $X_{ASA} \leq 0.2$, phenacetin is the outer layer.

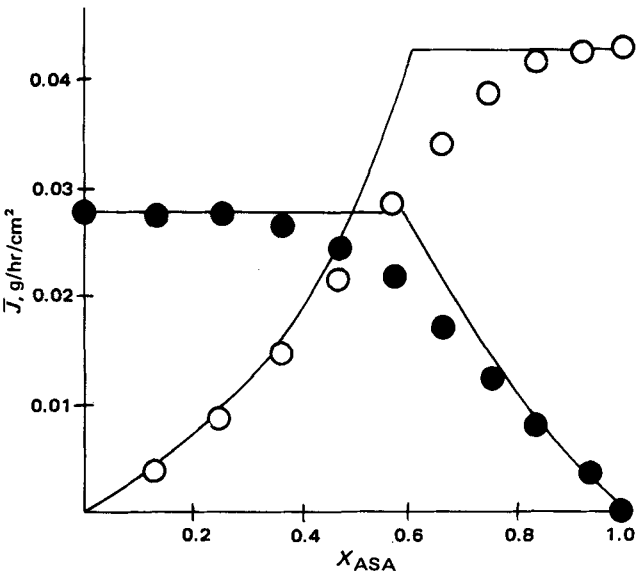

Figure 5—*Comparison of experimental fluxes of the components of aspirin–salicylic acid spheres with a bulk density of 1.4 g/cm³ of various compositions. Smooth curves are theoretical average fluxes. Key: ○, aspirin; and ●, salicylic acid.*

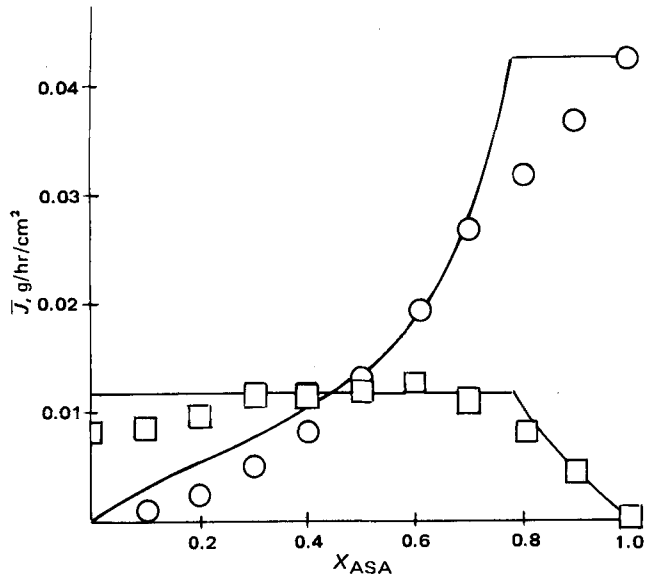

Figure 6—*Comparison of experimental fluxes of the components of aspirin–phenacetin spheres with a density of 1.4 g/cm³ of various compositions. Smooth curves are theoretical average fluxes. Key: ○, aspirin; and □, phenacetin.*

Two-Component, Interacting Solids—The general modeling discussed may be extended to include interacting solids. Consider the case in which components A and B react according to the reaction $A + B \rightleftarrows AB$ and the equilibrium constant, K, is expressed as:

$$K = \frac{\tilde{C}_{AB}}{\tilde{C}_A \tilde{C}_B} \qquad \text{(Eq. 16)}$$

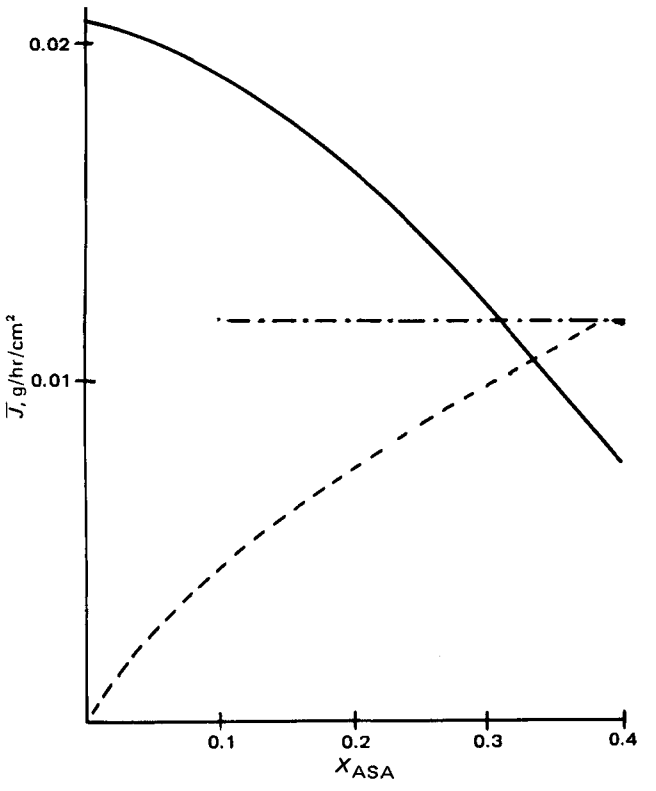

Figure 7—*Average fluxes of components of aspirin–caffeine–phenacetin spheres with a density of 1.5 g/cm³, X_{PH} = 0.5, and various compositions of aspirin and caffeine. Key: ---, aspirin; —, caffeine; and -·-·-, phenacetin.*

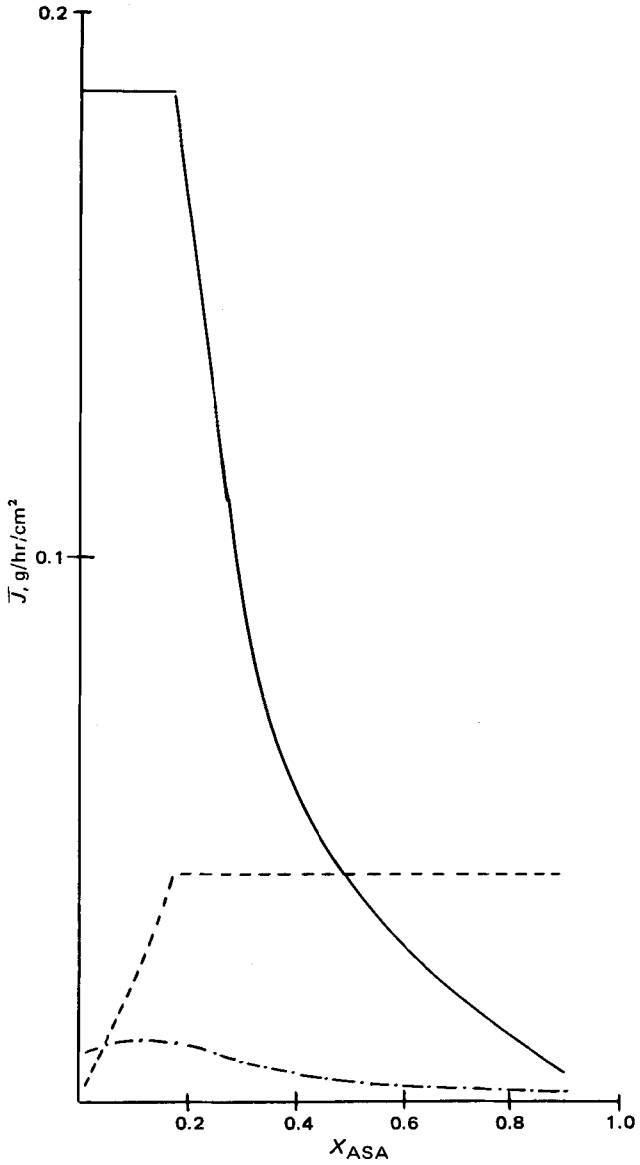

Figure 8—*Average fluxes of components of aspirin–caffeine–phenacetin spheres with a density of 1.5 g/cm³, X_{PH} = 0.05, and various compositions of aspirin and caffeine. Key: ---, aspirin; —, caffeine; and -·-·-, phenacetin.*

with the concentrations being expressed in molar concentrations as indicated by tildes.

The mass transfer may be expressed for the two-component, interacting system by:

$$-\frac{dW_A}{dt} = k_A S_A C_A^* + k_{AB} S_B M_A \tilde{C}_{AB}^* \qquad \text{(Eq. 17)}$$

$$-\frac{dW_B}{dt} = k_B S_B C_B^* + k_{AB} S_A M_B \tilde{C}_{AB}^* \qquad \text{(Eq. 18)}$$

where M_A and M_B are the molecular weights of A and B, respectively. Expressions for r_A and r_B may be found as discussed.

For the critical composition:

$$\frac{X_A}{X_B} = \frac{D_A C_A^* + M_A D_{AB} \tilde{C}_{AB}^*}{D_B C_B^* + M_B D_{AB} \tilde{C}_{AB}^*} \qquad \text{(Eq. 19)}$$

where $X_A + X_B = 1$.

Theoretically calculated values are drawn as solid lines in Fig. 9 in which the mass of a dissolving aspirin–caffeine sphere at 1 and 2 hr is plotted *versus* composition. The symbols represent experimental values. The model and experimental values are in good qualitative and quantitative agreement over the entire range of X_{ASA}.

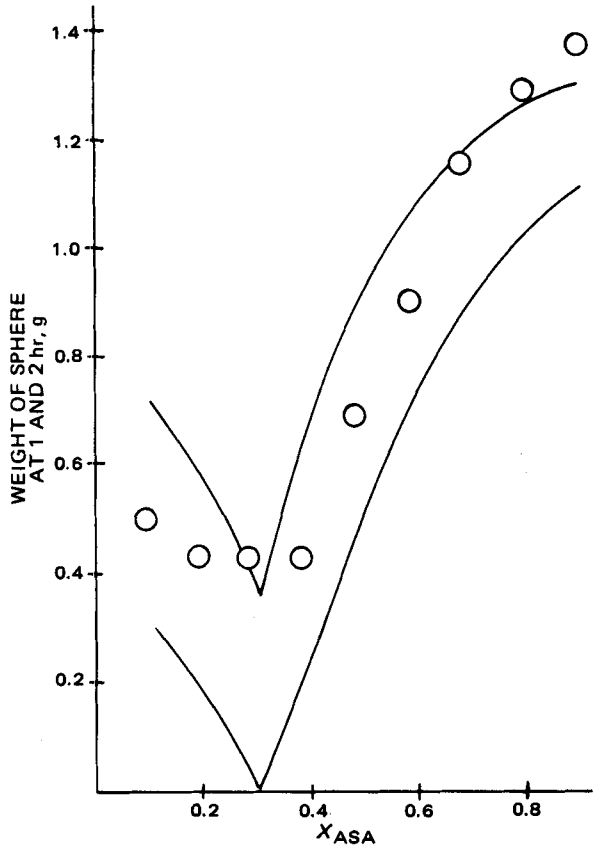

Figure 9—*Relation of composition to weight of a dissolving aspirin–caffeine sphere with a bulk density of 1.5 g/cm³. Smooth curves are theoretical, and points are experimental values. Key: upper curve, t = 1 hr; lower curve, t = 2 hr; and ○, experimental values at t = 1 hr.*

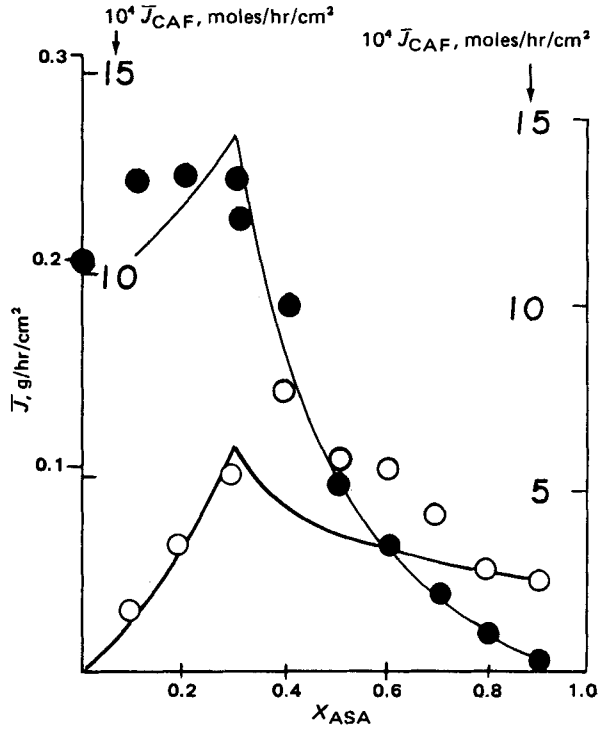

Figure 10—*Comparison of theoretical and experimental fluxes of the two components for an interacting two-component sphere with a bulk density of 1.5 g/cm³. Smooth curves are theoretical fluxes. Key: ○, aspirin; and ●, caffeine.*

The fluxes predicted by the model are compared to the experimentally determined fluxes in Fig. 10. The differences between interacting and noninteracting systems can be seen by comparing Fig. 10 with Figs. 5 and 6. There are no regions in a two-component, interacting system in which either flux is independent of the mass fraction. In addition, in a noninteracting system, the flux of aspirin can not exceed 0.043 g/hr/cm²; in interacting systems, the flux of aspirin can greatly exceed the noninteracting limit over a broad range of X_{ASA} values.

Three-Component Systems with Two Components Interacting—If a third component, I, is added to the two-component, interacting system, then in addition to Eqs. 17 and 18, an equation for mass transfer of I must be considered, *i.e.*:

$$-\frac{dW_I}{dt} = k_I S_I C_I^* \qquad \text{(Eq. 20)}$$

The expressions for the critical composition for this system are:

$$\frac{X_A}{X_B} = \frac{D_A C_a^* + M_A D_{AB} \tilde{C}_{AB}^*}{D_B C_B^* + M_B D_{AB} \tilde{C}_{AB}^*} \qquad \text{(Eq. 21)}$$

and:

$$\frac{X_I}{X_B} = \frac{D_I C_I^*}{D_B C_B^* + M_B D_{AB} \tilde{C}_{AB}^*} \qquad \text{(Eq. 22)}$$

where $X_I + X_A + X_B = 1$.

The equilibrium constant for the 1:1 aspirin–caffeine complex was reported to be 17.4 liters/mole (9). The hypothetical fluxes for each component of an aspirin–caffeine–phenacetin solid are shown in the remaining plots (see *Appendix*). The model for three components with two components interacting is plotted in Figs. 11 and 12, and it may be compared to Figs. 7 and 8 in which no interaction was hypothetically assumed between aspirin and caffeine. For $X_{PH} \geq 0.1$, the general shapes of the flux curves are similar (Fig. 11); however, for $X_{PH} \leq 0.1$, the effects of complexation are apparent (Fig. 12).

Due to caffeine–aspirin complexation, the flux of aspirin may be greater than in the hypothetical noninteracting case. In addition, for the inter-

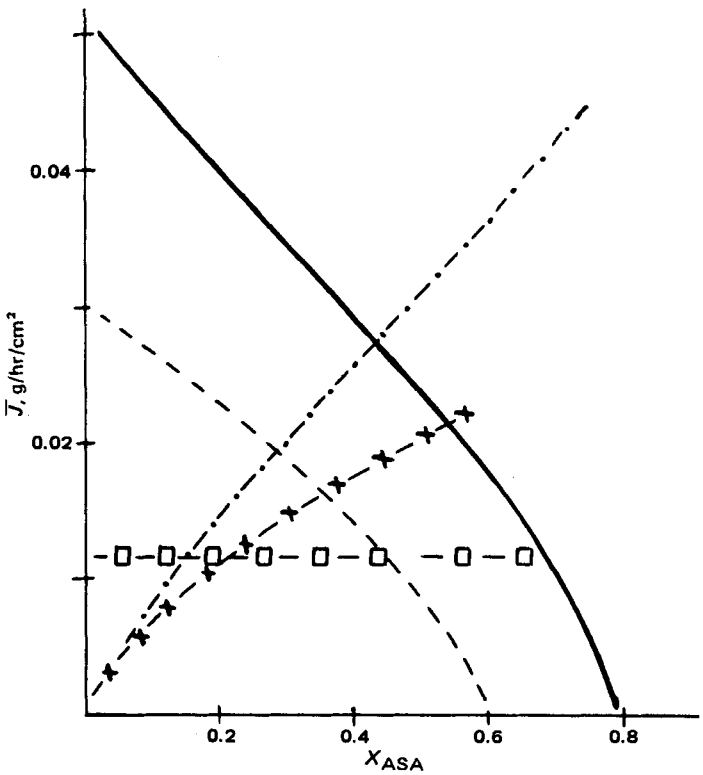

Figure 11—*Theoretical average fluxes of components of aspirin–caffeine–phenacetin spheres with a bulk density of 1.5 g/cm³, $X_{PH} \geq 0.1$, and various compositions of aspirin and caffeine. The hypothetical noninteracting case for this system is given in Fig. 7. Key: —, caffeine at $X_{PH} = 0.2$; - - -, caffeine at $X_{PH} = 0.4$; —·—, aspirin at $X_{PH} = 0.2$; ×–×–, aspirin at $X_{PH} = 0.4$; and □–□–, phenacetin at $X_{PH} = 0.2$ and $X_{PH} = 0.4$.*

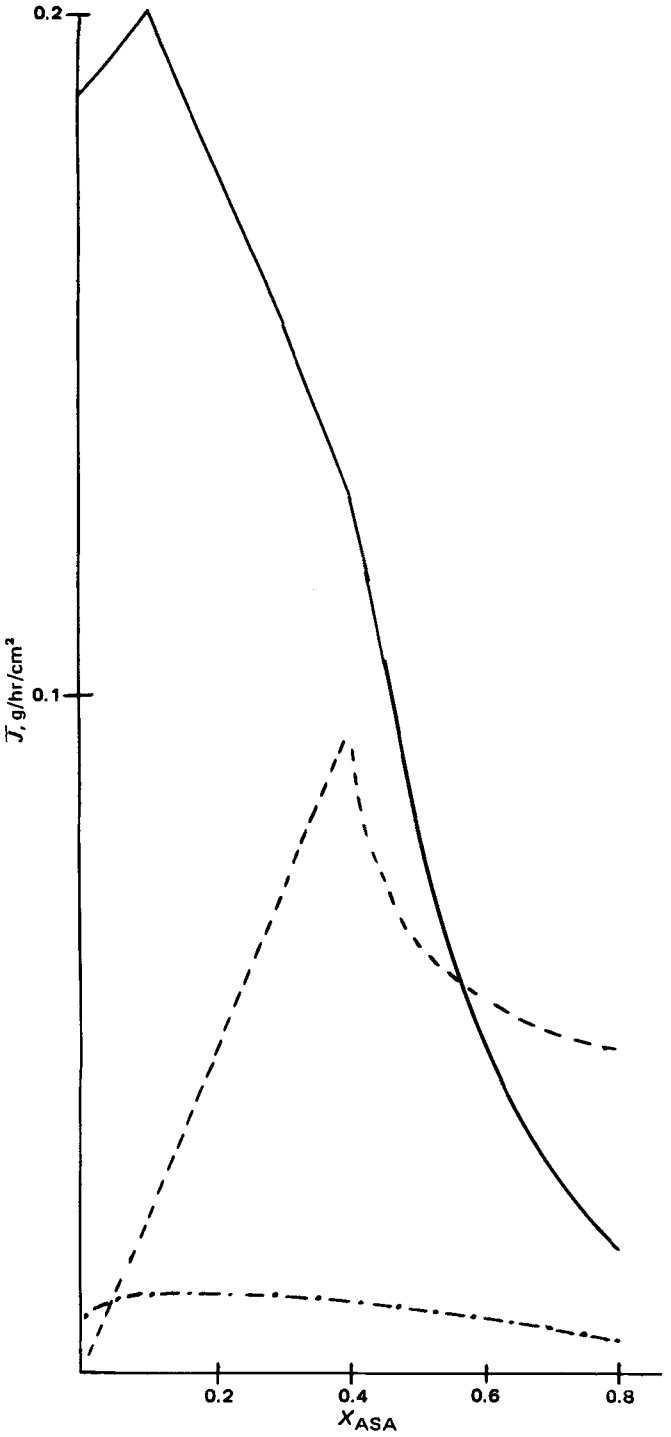

Figure 12—*Theoretical average fluxes of components of aspirin–caffeine–phenacetin spheres with a bulk density of 1.5 g/cm³, X_{PH} = 0.05, and various compositions of aspirin and caffeine with complexation. Key: ---, aspirin; —, caffeine; and -·-·-, phenacetin.*

acting case, three distinct regions occur as shown in Fig. 12. For $X_{ASA} \geqq 0.4$, aspirin forms the outer shell, and the fluxes of all three components decrease with increases in X_{ASA}. For $0.1 \leqq X_{ASA} \leqq 0.4$, phenacetin comprises the outer shell, and the flux of phenacetin remains constant while the flux of aspirin increases and the flux of caffeine decreases as X_{ASA} is greater. Caffeine forms the outer shell for $X_{ASA} \leqq 0.1$, and the fluxes of all three components increase as X_{ASA} is greater.

The experimental data for the three-component, interacting system (Table II) are comparable with reasonable qualitative agreement to the theoretical values in the remaining figures. In Fig. 13 with equal mole fractions of aspirin and phenacetin, the flux of caffeine is shown to be an

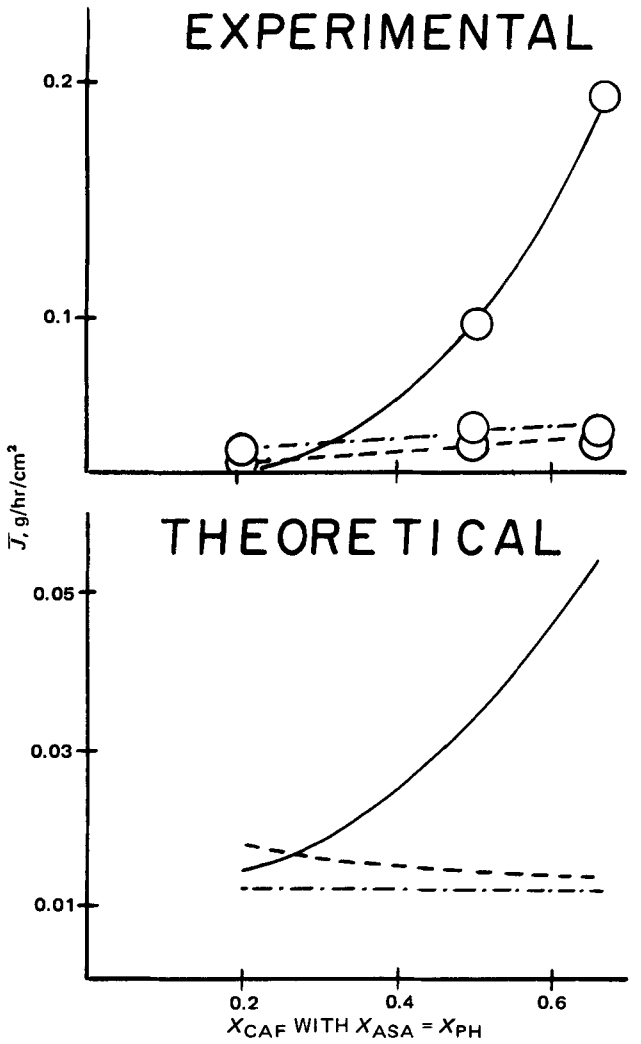

Figure 13—*Theoretical average and experimental fluxes of each component in a three-component, interacting system with equal mole fractions of aspirin and phenacetin. Densities are given in Table II. Key: ---, aspirin; —, caffeine; and -·-·-, phenacetin.*

increasing function of the mole fraction of caffeine; however, the fluxes of aspirin and phenacetin are relatively insensitive to the mole fraction of caffeine.

In Fig. 14 with equal mole fractions of aspirin and caffeine, the fluxes of aspirin and caffeine decrease exponentially as the mole fraction of phenacetin is increased, while the flux of phenacetin is less sensitive to change in the fraction of phenacetin. As shown in Fig. 15 with equal mole fractions of caffeine and phenacetin, the flux of aspirin increases as the mole fraction of aspirin increases, but the flux of caffeine decreases as the mole fraction of aspirin increases.

APPENDIX

The mathematics of the calculation of the fluxes is illustrated for a three-component solid with two interacting components.

The equations for the flux of the dissolution of aspirin (ASA)–caffeine (CAF)–phenacetin (PH) solids with an interaction between the aspirin and caffeine are obtained from Eqs. 7 and 8 using Eqs. 17, 18, and 20 (see text for definitions):

$$J_{ASA}(t) = k_{ASA}\frac{S_{ASA}}{S_{PH}}C^{\cdot}_{ASA} + k_{ASA\text{-}CAF}\frac{S_{ASA}}{S_{PH}}M_{ASA}\check{C}^{\cdot}_{ASA\text{-}CAF} \quad \text{(Eq. A1)}$$

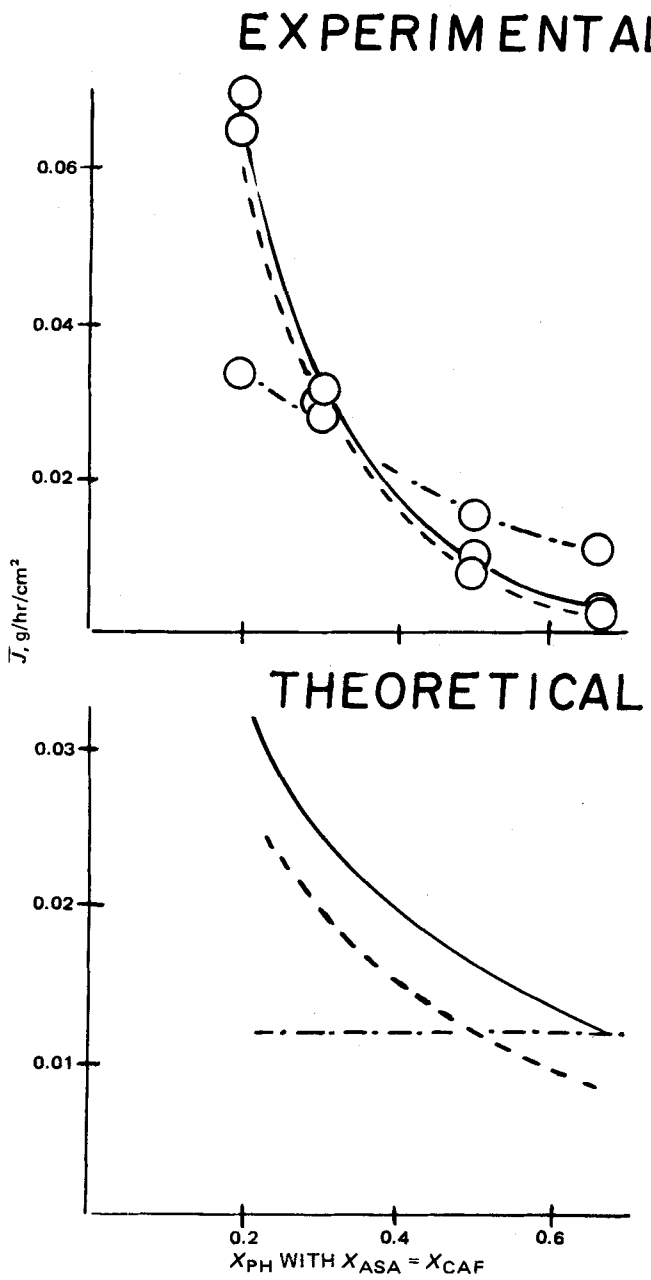

Figure 14—*Theoretical average and experimental fluxes of each component in a three-component, interacting system with equal mole fractions of aspirin and caffeine. Densities are given in Table II. Key: ---, aspirin; —, caffeine; and —·—, phenacetin.*

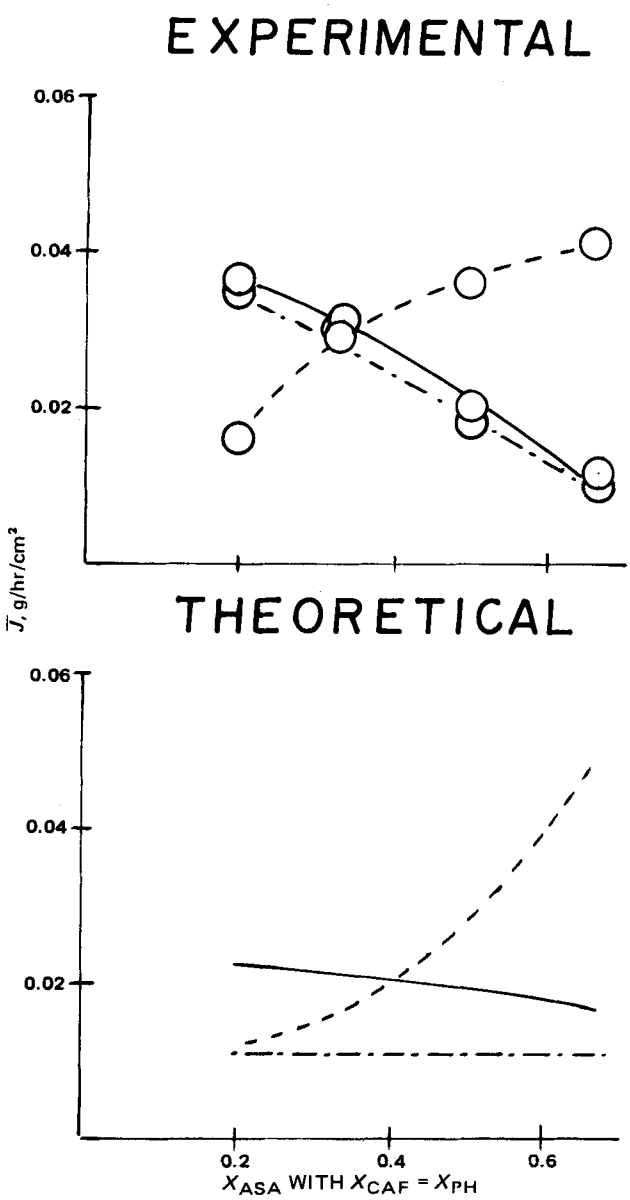

Figure 15—*Theoretical average and experimental fluxes of each component in a three-component, interacting system with equal mole fractions of caffeine and phenacetin. Densities are given in Table II. Key: ---, aspirin; —, caffeine; and —·—, phenacetin.*

$$J_{CAF}(t) = k_{CAF}\frac{S_{CAF}}{S_{PH}}C^{*}_{CAF} + k_{ASA\text{-}CAF}\frac{S_{CAF}}{S_{PH}}M_{CAF}\tilde{C}^{*}_{ASA\text{-}CAF} \quad \text{(Eq. A2)}$$

$$J_{PH}(t) = k_{PH}C^{*}_{PH} \quad \text{(Eq. A3)}$$

When phenacetin is the outer layer:

$$k_{ASA} = \frac{D_{ASA}}{h + r_{PH} - r_{ASA}} \quad \text{(Eq. A4)}$$

$$k_{CAF} = \frac{D_{CAF}}{h + r_{PH} - r_{CAF}} \quad \text{(Eq. A5)}$$

$$k_{PH} = \frac{D_{PH}}{h} \quad \text{(Eq. A6)}$$

and:

$$S_{ASA} = 4\pi r^2_{ASA} \quad \text{(Eq. A7)}$$

$$S_{CAF} = 4\pi r^2_{CAF} \quad \text{(Eq. A8)}$$

$$S_{PH} = 4\pi r^2_{PH} \quad \text{(Eq. A9)}$$

For the experimental conditions at 25°, the diffusivities and solubilities are given in Table III. The film thickness, h, was determined experimentally to be 30×10^{-4} cm, and the equilibrium constant for a 1:1 aspirin–caffeine complex was taken as 17.4 liters/mole. With the use of these physical parameters and Eqs. A4–A9, Eqs. A1–A3 can be written as:

$$J_{ASA}(t) = \left(\frac{9.76 \times 10^{-8}}{30 \times 10^{-4} + r_{PH} - r_{ASA}}\right)\left(\frac{r_{ASA}}{r_{PH}}\right)^2 \text{g/cm}^2\text{/sec} \quad \text{(Eq. A10)}$$

$$J_{CAF}(t) = \left(\frac{2.22 \times 10^{-7}}{30 \times 10^{-4} + r_{PH} - r_{CAF}}\right)\left(\frac{r_{CAF}}{r_{PH}}\right)^2 \text{g/cm}^2\text{/sec} \quad \text{(Eq. A11)}$$

$$J_{PH}(t) = 3.3 \times 10^{-6}\ \text{g/cm}^2\text{/sec} \quad \text{(Eq. A12)}$$

As shown by these equations, the fluxes are dependent on the indi-

vidual radii. The equations describing the radii are obtained from Eq. 6:

$$-\frac{dr_{ASA}}{dt} = \frac{D_{ASA}C^*_{ASA} + D_{ASA\text{-}CAF}M_{ASA}\tilde{C}^*_{ASA\text{-}CAF}}{(h + r_{PH} - r_{ASA})X_{ASA}\rho} \quad \text{(Eq. A13)}$$

$$-\frac{dr_{CAF}}{dt} = \frac{D_{CAF}C^*_{CAF} + D_{ASA\text{-}CAF}M_{CAF}\tilde{C}^*_{ASA\text{-}CAF}}{(h + r_{PH} - r_{CAF})X_{CAF}\rho} \quad \text{(Eq. A14)}$$

$$-\frac{dr_{PH}}{dt} = \frac{D_{PH}C^*_{PH}}{hX_{PH}\rho} \quad \text{(Eq. A15)}$$

where:

$$X_{PH} + X_{ASA} + X_{CAF} = 1 \quad \text{(Eq. A16)}$$

At 25°, the equations can be written as:

$$-\frac{dr_{ASA}}{dt} = \frac{9.76 \times 10^{-8}}{(30 \times 10^{-4} + r_{PH} - r_{ASA})X_{ASA}\rho} \text{ cm/sec} \quad \text{(Eq. A17)}$$

$$-\frac{dr_{CAF}}{dt} = \frac{2.22 \times 10^{-7}}{(30 \times 10^{-4} + r_{PH} - r_{CAF})X_{CAF}\rho} \text{ cm/sec} \quad \text{(Eq. A18)}$$

$$-\frac{dr_{PH}}{dt} = \frac{3.33 \times 10^{-6}}{X_{PH}\rho} \text{ cm/sec} \quad \text{(Eq. A19)}$$

These equations are coupled (r_{ASA} is a function of r_{PH}, *etc.*). For given values of X_i and ρ, these equations can be solved simultaneously to yield r_{ASA}, r_{CAF}, and r_{PH} as a function of time. A fourth-order Runge–Kutta procedure (8) was used in this study to solve these equations. When the radii are evaluated, the instantaneous fluxes may be calculated from Eqs. A10–A12. The average fluxes may be calculated using Eq. 12.

The equations describing the cases in which either aspirin or caffeine is the outer layer can be obtained similarly. The equations describing the hypothetical case in which aspirin and caffeine do not interact are obtained by setting $\tilde{C}^*_{ASA\text{-}CAF}$ to zero in these equations.

REFERENCES

(1) E. Nelson, *J. Am. Pharm. Assoc., Sci., Ed.*, **46**, 607 (1957).

(2) M. Gibaldi and H. Weintraub, *J. Pharm. Sci.*, **57**, 832 (1968).

(3) W. I. Higuchi, N. A. Mir, and S. J. Desai, *ibid.*, **54**, 1405 (1965).

(4) S. A. Shah and E. L. Parrott, *ibid.*, **65**, 1784 (1976).

(5) E. L. Parrott, D. E. Wurster, and T. Higuchi, *J Am. Pharm. Assoc., Sci. Ed.*, **44**, 269 (1955).

(6) R. J. Braun and E. L. Parrott, *ibid.*, **61**, 175 (1972).

(7) S. A. Shah, Ph.D. thesis, University of Iowa, Iowa City, Iowa, 1975.

(8) B. Carnahan, H. A. Luther, and J. O. Wilkens, "Applied Numerical Methods," Wiley, New York, N.Y. 1969, pp. 361–365.

(9) T. Higuchi and D. A. Zuck, *J. Am. Pharm. Assoc., Sci. Ed.*, **42**, 138 (1953).

ACKNOWLEDGMENTS

Abstracted in part from a dissertation submitted by S. A. Shah to the University of Iowa in partial fulfillment of the Doctor of Philosophy degree requirements.

Reversed-Phase High-Pressure Liquid Chromatographic Analysis of Sulconazole in Plasma

M. FASS ˣ, B. ZARO, M. CHAPLIN, and S. MATIN

Received June 2, 1980, from *Syntex Research, Palo Alto, CA 94304.* Accepted for publication May 12, 1981.

Abstract □ A sensitive and specific analytical method for the measurement of sulconazole in plasma is described. The compound was extracted from plasma at pH 10 with hexane–methylene chloride. Samples were subjected to high-pressure liquid chromatography (HPLC) using an acetonitrile–phosphate buffer mixture as the mobile phase. The components of interest were measured using a variable-wavelength detector at 229 nm. Sulconazole concentrations of ≥0.5 μg/ml can be measured with confidence using this method. Linear calibration curves were constructed over the concentration range of 0.5–5 μg/ml for sulconazole from dog plasma. A dog was administered a single oral 1000-mg dose of tritiated sulconazole nitrate; total plasma radioactivity and sulconazole plasma levels determined by HPLC are reported.

Keyphrases □ Sulconazole—reversed-phase high-pressure liquid chromatographic analysis in plasma □ High-pressure liquid chromatography—analysis of sulconazole in plasma □ Antifungal agents—sulconazole, reversed-phase high-pressure liquid chromatographic analysis.

Sulconazole nitrate, 1-[β-(4″-chlorobenzylthio)-2′, 4′-dichlorophenethyl]imidazole mononitrate (I), is a potential new antimycotic agent[1] developed for human use. Since it is necessary to conduct animal toxicity studies supported by plasma level data for new drugs, a sensitive and specific analytical method was developed.

A high-pressure liquid chromatographic (HPLC) method for the determination of econazole, a structural analog of sulconazole, was described previously (1). Direct application of this extraction–injection method to sulconazole analysis provided unsatisfactory chromatography. Interfering peaks at the retention time of the compounds of interest were observed, and laborious distillation of ether prior to extraction to remove peroxides did not prevent random oxidative degradation of sulconazole.

This paper describes a reversed-phase HPLC method for the measurement of sulconazole in plasma using a structurally related analog as the internal standard. The method was applied to the measurement of sulconazole in the plasma of a dog given a single oral dose of 1000 mg of tritiated sulconazole nitrate.

EXPERIMENTAL

Reagents and Materials—All solvents[2] were distilled-in-glass and liquid chromatography grade. All chemicals[1], available in-house, were analytical grade and were used without further purification. Inorganic reagents were prepared in purified water[3]. Standard solutions of sulconazole were prepared in methanol at the following concentrations: 40 μg/ml (stock solution) and 20, 16, and 4 μg/ml (spiking solutions). The internal standard solution was prepared in methanol at a concentration of 100 μg/ml. Solutions were stored at 4°. Standard solutions were prepared every 2 weeks.

[1] Syntex, Palo Alto, Calif.

[2] Burdick & Jackson Laboratories, Muskegon, Mich.

[3] Milli Q System, Millipore Corp., Bedford, Mass.

0022-3549/81/1200-1338$01.00/0